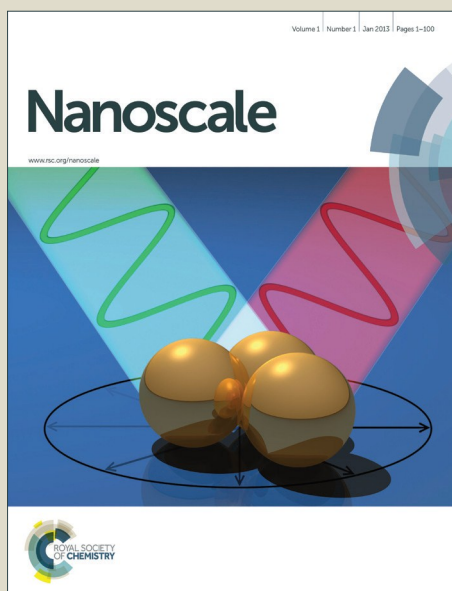


# Nanoscale

Accepted Manuscript



This is an *Accepted Manuscript*, which has been through the Royal Society of Chemistry peer review process and has been accepted for publication.

*Accepted Manuscripts* are published online shortly after acceptance, before technical editing, formatting and proof reading. Using this free service, authors can make their results available to the community, in citable form, before we publish the edited article. We will replace this *Accepted Manuscript* with the edited and formatted *Advance Article* as soon as it is available.

You can find more information about *Accepted Manuscripts* in the [Information for Authors](#).

Please note that technical editing may introduce minor changes to the text and/or graphics, which may alter content. The journal's standard [Terms & Conditions](#) and the [Ethical guidelines](#) still apply. In no event shall the Royal Society of Chemistry be held responsible for any errors or omissions in this *Accepted Manuscript* or any consequences arising from the use of any information it contains.

## Nanoparticle mechanics: deformation detection via nanopore resistive pulse sensing

Armin Darvish<sup>a,b</sup>, Gaurav Goyal<sup>a,b</sup>, Rachna N. Arora<sup>c</sup>, Ramalingam V. K. Sundaram<sup>a,c</sup>, Kidan Lee<sup>d</sup>,  
Chi Won Ahn<sup>e</sup>, Ki-Bum Kim<sup>d</sup>, Petia M. Vlahovska<sup>f</sup> and Min Jun Kim<sup>a,b\*</sup>

Solid-state nanopores have been widely used in the past for single-particle analysis of nanoparticles, liposomes, exosomes and viruses. The shape of soft particles, particularly liposomes with a bilayer membrane, can be greatly different inside nanopores compared to bulk solution as the electric field inside nanopores can cause liposome electrodeformation. Such deformations can compromise size measurement and characterization of particles, but are often neglected in nanopore resistive pulse sensing. In this paper, we investigated the deformation of various liposomes inside nanopores. We observed a significant difference in resistive pulse characteristics between soft liposomes and rigid polystyrene nanoparticles especially at higher applied voltages. We used theoretical simulations to demonstrate that the difference can be explained by shape deformation of liposomes as they translocate through nanopores. Comparing our results with the findings from electrodeformation experiments, we demonstrated that the rigidity of liposomes can be qualitatively compared using resistive pulse characteristics. This application of nanopores can provide new opportunities to study mechanics at nanoscale, to investigate properties of great value in fundamental biophysics and cellular mechanobiology, such as virus deformability and fusogenicity, and in applied sciences for designing novel drug/gene delivery systems.

---

<sup>a.</sup> School of Biomedical Engineering, Science and Health Systems, Drexel University, Philadelphia, PA 19104, United States

<sup>b.</sup> Department of Mechanical Engineering and Mechanics, Drexel University, Philadelphia, PA 19104, United States.

<sup>c.</sup> Department of Biochemistry and Molecular Biology, Drexel University College of Medicine, Philadelphia, PA 19102, United States.

<sup>d.</sup> Department of Materials Science and Engineering, Seoul National University, Seoul 151-742, Korea.

<sup>e.</sup> Department of Nano-Structured Materials Research, National Nanofab Center at Korea Advanced Institute of Science and Technology, Daejeon 305-806, Korea.

<sup>f.</sup> School of Engineering, Brown University, Providence, RI 02912, United States.

Electronic Supplementary Information (ESI) available: Supplementary figures; Signal Processing and Event Detection; Multiphysics Simulation in COMSOL

## Introduction

Solid-state nanopores were developed almost a decade ago as an alternative to protein nanopores<sup>1</sup> for next-generation sequencing of DNA molecules<sup>2</sup>, but in recent years they have drawn significant attention as a bioanalytical tool<sup>3</sup> to study various analytes including nucleic acids<sup>4-7</sup>, proteins<sup>8-11</sup>, viruses<sup>12-14</sup>, and nanoparticles<sup>15-18</sup>. The key sensing paradigm is to monitor ionic current through a nanopore in a thin film (Figure 1a) that separates two chambers (*cis* and *trans* chambers) (Figure 1b). The nanopore behaves as an ohmic resistance and the baseline ionic current through the pore,  $I_0$ , is determined by the size and shape of the pore and the ionic strength of the electrolyte solutions. Once analytes (molecules or particles) are added in the solution, they are transported through the pore by diffusion and electrokinetic forces. Presence of a particle inside the pore (Figure 1b), changes the resistance of the pore and causes unique modulation of the ionic current (resistive pulse or current blockade event) (Figure 1c). The amplitude of a single resistive pulse,  $\Delta I$ , and the translocation time,  $\Delta T$ , (Figure 1d) can be related to the physical properties (e.g. morphology and surface charge) of a single particle.

In the past few years, there has been a growing interest for using nanopores to characterize soft nanoparticles such as vesicles<sup>19, 20</sup>, viruses<sup>12, 21</sup>, viral capsids<sup>22</sup> and exosomes<sup>23</sup>, but to the best of our knowledge their morphology inside nanopores has not been addressed. Several groups have already demonstrated that forces inside nanopores<sup>24</sup> can stretch DNA molecules<sup>25</sup> and unfold proteins<sup>26-30</sup>. In fact force-deformation relationship has been used to study biophysical characteristics of single molecules, but the effects on larger particles are poorly understood. Few studies have addressed deformation of nanoparticles<sup>31</sup> and liposomes<sup>32</sup> in a nanopore due to osmotic or hydrostatic pressure, however electrodeformation of soft particles in a nanopore has mostly been ignored.

Electrodeformation, the deformation of vesicles under the influence of electric fields, is a well-studied phenomenon and has been previously used for mechanical characterization of microvesicles<sup>33, 34</sup> and

cells<sup>35-37</sup>. When vesicles pass through a nanopore, they experience a strong electric field, a process analogous to application of a DC pulse. As strong DC pulses can deform vesicles<sup>34, 38, 39</sup>, liposome deformation inside nanopores is expected. In fact, we recently reported a voltage-dependent behavior in resistive pulse signal of nanoscale liposomes<sup>40</sup>, which led us to the hypothesis that electrodeformation occurs inside nanopores.

In this paper we use ~100 nm liposomes as model analytes to study the electrodeformation phenomena inside nanopores. The main objective is to better understand the underlying mechanism of deformation, describe the shape of the deformed vesicles. Furthermore, by varying the lipid composition, we fabricated liposomes of different rigidity, to obtain a more comprehensive understanding of vesicle deformation and its correlation with lipid structure of the vesicles. Understanding deformation properties of different liposomes allows comparing their elastic properties. While the main focus here is on demonstrating proof-of-the-concept experiments and not quantitative measurements of biophysical properties, we believe that our findings can potentially transform nanopores into a novel analytical tool to study biophysical properties of nanoscale vesicles such as viruses, exosomes, liposomes, etc.

## Results and discussion

We used a round cylindrical nanopore, 250 nm in diameter, drilled in a 200 nm thick silicon nitride membrane by using focused ion beam (FIB), to compare translocation dynamics of various soft and rigid nanoparticles. For soft nanoparticles, we used liposomes prepared by the extrusion of varied lipid solutions. Particularly, we compared the translocation events of four liposome samples: 1,2-Dioleoyl-sn-glycero-3-phosphocholine (DOPC), 1-palmitoyl-2-oleoyl-sn-glycero-3-phosphocholine (POPC) as well as liposomes made out of 1:2 molar ratio of cholesterol and DOPC (DOPC/Ch) or POPC (POPC/Ch). For rigid particles we used two different samples of polystyrene nanoparticles, ~120 nm (NP120) and ~75 nm (NP75) in diameter, respectively. Figure 2 shows the size distribution of all six samples measured by

dynamic light scattering (DLS) and representative Transmission Electron Microscopy (TEM) images of each particle population. As can be seen, the liposomes are generally comparable in size even though they are heterogeneous in nature with a positive skewness observed in DLS measurements. We believe this skewness is a result of aggregation caused by the salt concentration in phosphate buffer saline (PBS) solution (140 mM KCl and pH = 7.4), which was used to imitate the physiological conditions. Nanopore resistive pulse measurements were done shortly after DLS measurements to avoid further aggregation. TEM images of all samples show very round spherical particles. While the size of rigid polystyrene nanoparticles in TEM images is comparable to DLS measurements, liposomes seem smaller under TEM due to liposome dehydration as they are dried in preparation for TEM imaging. Since nanopore experiments are done in solution, where liposomes are fully hydrated, we use the size measured by DLS as particles' true size in solution.

Examples of current traces recorded for each sample is shown in Supplementary Figure S1. All liposomes samples and NP75 nanoparticles showed translocation events with minimal clogging events. In contrast, NP120 particles showed frequent pore clogging, as shown in Supplementary Figure S1 and S2. Even though the clogged pore could be declogged by reversing the voltage or applying a cyclic biphasic voltage pulse of up to 4V of peak-to-peak height, we found it difficult to collect as many translocation events for NP120 as for other samples (Supplementary Figure S2a). Therefore, the NP120 data are excluded from our main discussion to avoid possible discrepancies caused by pore clogging and low statistics. The results for NP120 after filtering out all the partial clogging events are included in the Supplementary Figure S2 and we will refer to it if it helps the discussion. For all other samples, we were able to collect over 2000 translocation events at a range of applied voltages from 0.2V to 1V and replicated the experiments twice using the same pore shown in Figure 1a. To avoid cross contamination, we flushed the fluidic cells with bleach, water and ethanol three times and cleaned the nanopore chip in hot piranha solution for 5-10 minutes. The pore conductance was measured before each experiment to

ensure the pore condition remains the same and current trace with PBS was monitored to confirm no cross contamination between different samples.

**The resistive pulse characteristics show a significant difference between soft liposomes and rigid nanoparticles.**

As illustrated in Figure 3a, the most probable  $\Delta I$  values of liposomes remained almost constant regardless of the applied voltage, but increased linearly for NP75. This is similar to what we observed previously<sup>40</sup>, however, in our previous work, we had to use a low ionic strength buffer to maintain liposomes' integrity. At low ionic strengths, the translocation events can look very different since the effect of surface charges becomes significant<sup>17</sup>. Hence, we could not rule out the possible effect of experimental conditions in our previous work. Here, we prepared all liposomes in PBS buffer and compared them to rigid nanoparticles dispersed in PBS as well. The different trends in  $\Delta I$  vs. applied voltage (Figure 3a) between liposomes and rigid particles can therefore be truly attributed to the behavior of liposomes and not the effect of ionic strength. We further discuss several possible scenarios to ensure that the difference is caused by liposome shape deformation and not translocation dynamics or electrical signal detection.

**Liposome capacitance does not explain their resistive pulse characteristics.**

Unlike rigid nanoparticles liposomes act as a capacitor. Since the lipid bilayer is impermeable to ions, in the presence of electric field free charges brought by conduction from the bulk accumulate on the membrane surfaces and give rise to a potential difference across the membrane. Thus, just like a capacitor, liposomes can take part in the conduction process as they draw current until fully charged. In other words, while liposomes charge, the current drop would not be as intense as it is for a pure resistor (i.e. solid particles). For an initially charge-free spherical liposome with known radius,  $a$ , the capacitor charging time,  $t_m$ , can be calculated from the equation<sup>39</sup>:

$$t_m = aC_m \left( \frac{1}{\sigma_{in}} + \frac{1}{2\sigma_{ex}} \right) \quad (1)$$

Where  $C_m$  is the membrane capacitance and  $\sigma_{in}$  and  $\sigma_{ex}$  are the solution conductivities inside and outside the liposome, respectively. Under the conditions of our experiments, with  $\sigma_{in}$  and  $\sigma_{ex}$  equal to  $1.489 \text{ S.m}^{-1}$ ,  $C_m \sim 0.01 \text{ F.m}^{-2}$ <sup>33</sup>, and  $a \sim 100\text{-}125 \text{ nm}$ , the capacitor charging time of the membrane is estimated to be  $\sim 0.5 \text{ ns}$ . The translocation time of liposomes through nanopores, as measured by full width at half maximum (FWHM) of the resistive pulse, is  $60\text{-}200 \text{ }\mu\text{s}$  (Figure 3b), which is four orders of magnitude larger than the capacitive charging time. In other words, the liposomes are almost instantaneously charged and the charging time would play no role in the pore conductance. In addition, at a sampling frequency of  $250 \text{ kHz}$  for current measurements, the temporal resolution is not sufficient to observe the effect of liposomes' capacitive charging. Hence, the difference in  $\Delta I$  trends between liposomes and rigid nanoparticles cannot be explained by the capacitive charging of liposomes.

**Translocation trajectories are not responsible for the observed current blockade trends.**

Another scenario to consider is the dependence of resistive pulse shape on particle trajectory in a low-aspect-ratio pore that was recently reported by Tsutsui *et al.*<sup>41</sup> Since the nanopore used in this work was  $200 \text{ nm}$  in length and  $250 \text{ nm}$  in diameter, it can be considered a low aspect ratio pore. As suggested by Tsutsui *et al.*<sup>41</sup>, an off-center translocation through the pore can cause current blockade events with larger amplitude than translocation through the center of the pore. These off-center translocations will have an asymmetric skewed shape with larger falling time than rising<sup>41</sup>. If increasing voltage in our experiments can force liposomes to go through the center of the pore, we can expect attenuated resistive pulse amplitudes, which can manifest as constant  $\Delta I$  when the increased baseline current at higher voltages is considered. We examined the shape of our resistive pulses for asymmetric events like those reported by Tsutsui *et al.*<sup>41</sup> Figure 3c illustrates an overlay of over 100 typical resistive pulses for DOPC, POPC and NP75 at low, mid and high range voltages. All the events are very symmetric, suggesting that the particles are passing through the center of the pore. In fact, the ratio of falling time

to rising time of the resistive pulse signals remains about 1 for all samples at all voltages as depicted in Figure 3d. Therefore, the voltage-dependent trend of liposomes current blockades cannot be explained by the trajectory of liposomes' translocation through the pore.

**The event detection algorithm does not bias the data at varied applied voltages.**

A major aspect of resistive pulse sensing is signal processing especially for event detection. The common practice is to use a threshold to separate translocation events from the baseline current. At lower applied voltages, the signal-to-noise ratio of resistive pulse signal reduces and therefore there is a chance that a portion of translocation events are missed in event detection algorithms due to poor signal-to-noise ratio. Theoretically it is possible to hypothesize a scenario where small particles go undetected at low applied voltages, while at increased voltages with better signal-to-noise ratios, their resistive pulse becomes apparent. In other words there is a chance that the event detection algorithms for solid-state nanopore signals are biased toward larger particles at low voltages. As a result of such bias, the distribution of  $\Delta I$  can shift to smaller values when the voltage is increased, and because the baseline current increases with voltage as well, such shift toward smaller values can produce an artifact similar to the constant  $\Delta I$  observed for liposomes. However, our results with smaller rigid nanoparticles, NP75, show that the event detection algorithm can perfectly pick up small  $\Delta I$  values almost two times smaller than the most probable  $\Delta I$  detected for liposomes at 0.2V. The baseline noise in all our experiments was comparable and we used an unbiased event detection algorithm by using the standard deviation of baseline noise (See Supplementary Information) to detect translocation events of all samples. Thus, the signal processing and event detection algorithms cannot be responsible for the observed trends in the data.

**The difference between soft and rigid particles is caused by liposome deformation.**

As discussed above, liposomes capacitance, translocation dynamics and event detection algorithms cannot explain the trends in our  $\Delta I$  data. Hence, the only possible explanation can be a change in shape

or size of liposomes at higher applied voltages. In fact, at the lowest applied voltage, 0.2V, the most probable  $\Delta I$  values (Figure 3a) are higher for liposomes as is expected from their larger size. In stark contrast, at 1V the  $\Delta I$  value of NP75 is  $\sim 3$  times higher than that of the liposomes, suggesting that the liposomes are undergoing significant deformation. Furthermore, larger NP120 rigid particles, that were comparable in size to liposomes (Figure 2), caused pore clogging much more frequently than liposomes (Supplementary Figures S1 and S2), confirming that liposomes do in fact undergo deformation as they translocate through the pore.

Next, we investigated the relationship between shape and resistive pulse magnitude to assess whether the shape of deformed liposomes can be inferred from their resistive pulse characteristics. Ignoring the surface effects, the relationship between resistive pulse and dimensions of a translocating globular particle with width (dimension perpendicular to pore axis),  $r$ , and length (dimension parallel to pore axis),  $l$ , can be described by<sup>8, 42</sup>:

$$\Delta I = I_0 \frac{\Lambda}{H_{eff} A_{pore}} \left[ 1 + f\left(\frac{r}{D_{pore}}, \frac{l}{H_{eff}}\right) \right] \quad (2)$$

Where  $\Delta I$  is the amplitude of the resistive pulse,  $I_0$  is the baseline current,  $\Lambda$  is the volume of the particle,  $H_{eff}$  is the effective length of the pore,  $A_{pore}$  is the cross section area of the pore and the term  $f(r/D_{pore}, l/H_{eff})$  represents a function of  $l$ ,  $r$ , pore diameter ( $D_{pore}$ ); and  $H_{eff}$ . Since the geometry of a solid-state nanopore does not change during the experiment, the terms that describe the pore geometry ( $H_{eff}$ ,  $A_{pore}$ ,  $D_{pore}$ ) are all constant. The particle's volume,  $\Lambda$ , is a function of particles' dimension and can be rewritten in terms of  $l$  and  $r$ . Thus, equation 2 can be simplified to:

$$\frac{\Delta I}{I_0} = f'(r, l) \quad (3)$$

In other words, the normalized current blockade ( $\Delta I/I_0$ ) is a function of the geometry of the translocating particle ( $l$  and  $r$ ). It is important to note that the  $\Delta I/I_0$  value does not depend on any

experimental conditions (such as applied voltage or electrolyte strength) and therefore can be used to infer the morphology of translocating analyte independent of the experimental conditions.

Although an analytical solution to equation 3 is not trivial to obtain, numerical simulations can be used to find the relationship between  $\Delta I/I_0$  and particles' aspect ratio ( $1/r$ ). Several groups including ours have previously used a continuum model to simulate the resistive pulse of a translocating analyte<sup>18, 43-45</sup>. These models use a finite element simulation to solve the coupled Poisson, Nernst-Planck and Navier-Stokes equations (PNPS). For example, Liu *et al.*<sup>18</sup> used such model to predict the open pore conductance of solid-state nanopores fabricated with different methods and Venta *et al.*<sup>44</sup> simulated the resistive pulse events due to translocation of gold spheres and nanorods through a small nanopore. Here we use a similar method to simulate resistive pulse events of elliptical and spherical particles in order to obtain a numerical solution for equation 3. Since general discussion of the assumptions, boundary conditions, validity and applications of the PNPS models for nanopore translocation experiments can be found elsewhere<sup>46, 47</sup>, we only discuss the specific details pertaining to our model here.

We used an axis-symmetric model with a cylindrical pore geometry 250 nm in diameter, similar to measured diameter under TEM (Figure 1a). Since we use a large pore with a low-aspect ratio of thickness (200 nm) to diameter (250 nm), the effect of the pore shape is negligible<sup>18</sup> and therefore we used a cylindrical shape with round edges. For the flow cells we used cylinders 2  $\mu\text{m}$  away from the pore on each side. Voltage bias, concentration and other boundary conditions were applied as described elsewhere<sup>18, 43, 44</sup>. Further details of the simulation procedure can be found at the methods section and the supplementary information.

Figure 4a shows the voltage drop across the nanopore when a bias of 1V is applied across the flow cell. The voltage drop is mainly confined within the nanopore, resulting in localized electric field as shown in Figure 4b. The magnitude of the simulated electric field ranges from 5 to 25 kV/cm for applied

voltages between 0.2V and 1V. The ionic current through the pore was calculated by integrating the total flow of ions through the cross section of the pore as described elsewhere<sup>43, 45</sup>. Figure 4c compares the experimentally measured pore conductance with the simulation results, showing a good agreement between the two. Once we confirmed that the model can accurately predict the open pore conductance, we placed an elliptical particle close to one boundary of the flow cell and moved it periodically through the pore axis. Figure 4d shows an example of an elliptical particle as it passes through the pore. The color gradient shows the strength of the electric field at an applied voltage of 1V when the particle is at the center of the pore. Black lines show the electric field lines. Red and yellow arrows show the flux of negative  $\text{Cl}^-$  and positive  $\text{K}^+$  ions, respectively. The presence of the particle inside the pore causes a drop in the simulated current by blocking the ion fluxes. The simulation was then repeated for elliptical particles of varied aspect ratios and the results are plotted in Figure 4e. Since the internal fluid in liposomes is incompressible, we can assume that the liposomes' volume remains constant. Therefore we used ellipsoids of constant volume and different aspect ratios. The amplitude of the simulated resistive pulse decreases as the ellipse goes from an oblate ( $l/r < 1$ ) to a sphere ( $l/r = 1$ ) to a prolate ( $l/r > 1$ ) geometry. In other words, the normalized current blockade ( $\Delta I/I_0$ ) should increase if a spherical particle is stretched in the direction perpendicular to the pore axis and drops if the particle is stretched parallel to the pore axis. Next, we repeated the simulation for particles of different width ( $r$ ), 50-200 nm, and varied aspect ratios (Figure 4f). The red dots in Figure 4f show the simulated  $\Delta I/I_0$  for these particles and the intermediate values were calculated by fitting a cubic polynomial function to obtain the gradient colored surface illustrated in Figure 4f. This 3D surface represents a numerical solution to equation 3 and can be used to predict the morphology of globular particles within nanopores.

**Liposome deformation is caused by the electric field in the pore and the morphologies are prolate ellipsoids.**

In order to compare our experimental data with the simulation results, first we calculated the normalized current blockade ( $\Delta I/I_0$ ) for each event and plotted the most probable value, calculated from the peak of respective histograms, for each sample at all applied voltages (Figure 5a). The  $\Delta I/I_0$  value remains constant at  $\sim 1.5\%$  for solid NP75 nanoparticles, suggesting that their shape was maintained as expected for rigid particles. For liposomes, however, the  $\Delta I/I_0$  decreases significantly, suggesting that the liposomes are going under deformation into prolate morphologies, i.e. they are getting stretched in the direction parallel to the pore axis. While deformation has been previously observed for other analytes including DNA<sup>24, 48</sup>, proteins<sup>28-30</sup> and polymers<sup>31, 49</sup> the best of our knowledge no one has studied liposome deformation inside nanopores. Even though, Holden *et al.*<sup>32</sup> reported liposome deformation in glass nanopores, their experiments were done with liposomes much larger than the aperture of the pore and therefore the deformation was attributed to confinement of liposomes and squeezing through the nanopore orifice. This is very different in term of the underlying physics from our observation, where liposomes were smaller than the pore diameter. Others have reported hydrogel deformation in a polymer nanopore<sup>31</sup> due to a drop in local pressure within the pore caused by the electroosmotic flow. Local pressure, however, cannot play a significant role in our experiments because in our low aspect ratio pore the surface effects are negligible and the pressure inside the pore approaches that of bulk solution. Thus, the mechanism for liposome deformation in our work is different from those previously reported for soft particles. It is necessary to consider the forces acting on liposomes inside nanopores to better understand the underlying mechanism of deformation. Several groups have addressed this issue, especially for DNA<sup>24</sup> and proteins<sup>50</sup>. In general, analyte translocation through the nanopore is a result of diffusion, electrophoresis and electroosmosis. The diffusion drift is caused by the concentration gradient across the pore. The electrophoresis is the result of electric force on charged species in an electric field. The electroosmosis arises from the Coulomb force on the electric double layer formed next to the charged surface of nanopores. The net force on the translocating analyte is therefore the resultant of

the actions of these three processes<sup>50</sup>. In case of charged species, such as DNA and proteins, the electroosmotic force and the electrophoretic force can act in opposite directions; hence it has been proposed that these forces can stretch the molecule by pulling it toward opposite directions<sup>24, 50</sup>. The liposomes we used in this work, however, are not charged at neutral pH and therefore the electrophoretic forces are negligible. As a result, the translocation is only facilitated by diffusion and electroosmosis (Figure 5b). When these two are acting in the same direction, they facilitate liposomes to overcome the entropic barrier of confinement inside nanopores and translocation events become much more frequent. In fact, translocation events were observed more frequently when liposomes were placed in the *trans* chamber rather than the opposite direction (Supplementary Figure S3). The data presented here were all collected for translocation from *trans* to *cis* chamber and therefore the forces acting on the liposomes were in the same direction. As a result, the stretching effect proposed for DNA and proteins cannot be applied to liposomes. Instead, the deformation is a direct result of electrodeformation, as is discussed below.

Electrodeformation and poration are well-established phenomena that have found applications in cell transfection<sup>51-54</sup> and in mechanical characterization of vesicles<sup>35, 55</sup> and cells<sup>56</sup>. A detailed discussion of electrodeformation and its underlying physics is beyond the scope of this paper and can be found elsewhere<sup>33, 57</sup>, but here we look into some of the recent works that explain the morphology of liposomes inside electric fields<sup>38, 39, 58</sup> and will compare conditions inside nanopores to those experiments to investigate whether liposome electrodeformation can occur as they translocate through nanopores. Strong DC fields ranging in magnitude from 2 kV/cm to >50 kV/cm have been shown to deform liposomes at both micro-<sup>36, 39</sup> and nanoscale<sup>59, 60</sup>. At microscale, where the shape of deformed liposomes can be imaged by a high-speed camera<sup>61, 62</sup>, liposomes deform into ellipsoids of varied aspect ratios depending on the experimental conditions. For liposomes filled with solutions of similar conductance to the bulk solution ( $\sigma_{in}/\sigma_{out} = 1$ ), the morphology is a prolate ellipsoid ( $l/r > 1$ )<sup>57</sup>. This is in

agreement with our results, where the drop in  $\Delta I/I_0$  at increased applied voltages (i.e. stronger fields) suggests deformation into a prolate ellipsoidal morphology. In fact, a liposome translocating through a nanopore undergoes an electric field of the shape shown in Figure 4b, which is essentially similar to applying a DC pulse on a stationary particle. Taking the translocation time (50-100  $\mu\text{s}$ ) into consideration, the nanopore translocation is analogous to applying a pulse of duration 50-100  $\mu\text{s}$  (or an AC field of 20-40 kHz) and magnitude of 5-25 kV/cm as shown in Figure 4b. Comparing these numbers with theoretical models that describe the morphology of the deformed liposomes<sup>57</sup> confirms a prolate morphology. While these theoretical models have been developed for microscale liposomes and may not directly be applicable at nanoscale, the general mechanisms and morphologies should be similar even at nanoscale. In fact, experimental data with liposomes comparable in size to our samples, have suggested that electrodeformation occurs at nanoscale<sup>59, 60</sup>. Even though, due to diffraction limits, the exact morphology cannot be imaged at nanoscale, complex optical absorption measurements have predicted that the deformed liposomes are prolate ellipses<sup>59</sup>. Thus, it is reasonable to conclude that liposomes will undergo electrodeformation as they pass through nanopores and their morphology should be prolate ellipsoids.

We used our numerical simulation results (Figure 4f) to estimate the effective aspect ratio of the deformed liposomes inside nanopores based on their normalized current blockade ( $\Delta I/I_0$ ) assuming that their shape is prolate ellipsoids. As it is shown in Figure 5c, we predict the aspect ratio of rigid NP75 to be  $\sim 1$  (i.e. a sphere) independent of the applied voltage. This confirms that our simulation is accurately modelling the resistive pulse. Considering that the only input in the simulation is the initial diameter of the particle, an output of aspect ratio equal to 1 is a good prediction for the shape of rigid particles. For liposomes, however, we see an increase in the aspect ratio (i.e. deformation to prolate shapes) as voltage is increased. However, the values for the effective aspect ratio are unexpectedly high especially at higher applied voltages. Generally, electrodeformation experiments report slightly prolate ellipsoids

with aspect ratios in the range of 1-1.5<sup>39, 59</sup>. But, our results show aspect ratios larger than 2 even at 0.3 V (despite the low field strength of ~6 kV/cm). We do not believe that the estimated effective aspect ratios are a true representative of the liposomes' exact morphology, but rather an indication of the extent of liposome deformation. It is important to understand that because of the complicated underlying physics inside nanopores, our estimation of liposome's exact morphology is not ideal. First, our numerical simulation assumes constant particle's volume, which should hold true as long as the liposomes do not porate or disintegrate. However, the high membrane curvature of nanoscale liposomes favors poration<sup>59</sup>, therefore loss of volume is possible due to electroporation. In addition, a porated liposome can take part in ionic conduction. Smaller volume and lower resistance due to poration will likely cause resistive pulses of smaller magnitudes than expected, hence higher aspect ratio predictions. Second, unlike electrodeformation experiments in bulk solution, in our experiments liposomes are confined inside the nanopore, which can have implications for liposome's shape. In fact pore-liposome interactions may amplify liposome deformation as adsorption on surfaces is known to flatten liposomes<sup>63, 64</sup>. There is even a possibility that liposomes hit the surface of nanopores and burst immediately<sup>64</sup> to form a bilayer on the pore surface<sup>65</sup>. We believe the latter is less likely because no significant shift in the baseline was observed with liposome translocation (Supplementary Figure S1). The shape of the current blockade events and the translocation times of the liposomes did not suggest any prolonged liposome-pore interactions, either. Yet, we cannot completely refute the possibility of liposomes pore interactions and its possible effects on liposomes' morphology. Furthermore, the presence of electroosmotic flow and the simple fact that liposomes are in translocation may have implications for their deformation. In addition, our aspect ratio prediction is based on the assumption that the most probable  $\Delta I/I_0$  corresponds (the peak in histograms of  $\Delta I/I_0$  distributions) to the most probable particle size (The peak in DLS measurements). However, the liposomes are heterogeneous in size with skewed distributions, which can result in varied levels of deformations for different

subpopulations within the sample. The bending rigidity of nanoscale liposomes are highly correlated to their membrane curvature<sup>66-68</sup>, which means that with the same applied force, larger particles will undergo more deformation. In other words, the deformation can further skew the  $\Delta I/I_0$  distribution, which may complicate the assumption that the most probable  $\Delta I/I_0$  corresponds to the average size. Finally, due to computational limitations, we have used a rather simplistic model that assumes an axisymmetric electric field around liposomes at steady-state conditions, which may not be a true representative of the conditions in our experiments. The nanopore was not perfectly circular and the dynamics of liposome deformation as it passes through nanopores may deviate from steady-state conditions. Importantly, our model did accurately predict the aspect ratio of larger NP120 rigid particles to be  $\sim 1$  as well (Supplementary Figure S2d), confirming that the larger size of the liposomes do not cause the difference seen in their aspect ratio prediction. As a result we conclude that the trend of increasing aspect ratios with applied voltage does in fact illustrate liposome deformation even though the actual values may be inaccurate for the reasons discussed above.

**Rigidity of different liposomes can be compared by their resistive pulse properties.**

Despite unexpectedly high estimated aspect ratios for liposomes, the comparative trends between various liposomes can still be of great value. For example, DOPC liposomes show more deformation (higher aspect ratios) than POPC based liposomes, which is in agreement with the fact that POPC bilayer has a higher bending rigidity<sup>69, 70</sup>. Furthermore, the effect of cholesterol on DOPC liposomes seems smaller than the effect on POPC liposomes. Up to 0.7 V, DOPC and DOPC/Ch liposomes show similar deformation behavior. At voltages above 0.7 V, the DOPC liposomes show more deformation, but due to the higher standard errors in these measurements; the difference between DOPC and DOPC/Ch is not significant. POPC liposomes on the other hand show more deformation compared to POPC/Ch at voltages above 0.3 V, which suggests that addition of cholesterol to POPC causes stiffening. These results are in agreement with the results from electrodeformation and other experiments. As

demonstrated by Henriksen *et al.*<sup>71</sup> addition of cholesterol to POPC liposomes increased their stiffness, which led to the belief that cholesterol has a universal stiffening effect on lipid bilayers. More recent experiments, however, have suggested that the effect is lipid specific<sup>72</sup> and in fact for DOPC liposomes, addition of cholesterol has no effect on particles bending rigidity. This has been confirmed in electrodeformation studies of DOPC microvesicles<sup>35</sup>. Therefore, our findings for the effect of cholesterol are in agreement with the findings in the literature and we can conclude that the trends in our data represent liposome electrodeformation. Hence, nanopores can be used to qualitatively compare the bending rigidity of liposomes.

One final point that we find worthy of discussion is the distributions of  $\Delta I$  values. As illustrated in Supplementary Figure S4 the distributions are very different for liposome vs. rigid nanoparticles. The  $\Delta I$  values for rigid polystyrene nanoparticles show a normal Gaussian distribution, which is expected for nanopore translocation events<sup>45, 73</sup>. However, the distributions are very positively skewed for all liposome samples. The skewness might be attributed to the fact that the liposome's size distributions were also skewed (Figure 2). But, the NP120 particles, which were skewed in DLS measurements as well, did not show skewness in  $\Delta I$  (See Supplementary Figure S2b). Thus the skewness may not necessarily be the result of particle size distribution. Interestingly, skewed  $\Delta I$  distributions have been increasingly observed over the past few years, and in most cases it is attributed to the shape of the translocating analyte and its orientation within the pore<sup>74</sup>. For example, unimodal positively skewed distributions similar to what we have observed here, was reported for bovine serum albumin and fibrinogen<sup>8</sup>. Although the authors did not discuss the  $\Delta I$  distribution, it is noteworthy that the shape of the translocating molecules in their work was also elliptical with high aspect ratios<sup>8</sup>. This is very intriguing because to the best of our knowledge it is the only other report with a unimodal positively skewed  $\Delta I$  distribution, and the morphology is similar to what we expect for deformed liposomes. As suggested recently<sup>74</sup>, the resistive pulse signal and the distributions of pulse characteristics can be used to

accurately characterize the shape of a single protein molecule. Similar analysis for larger particles such as liposomes can be of great interest in order to better predict the shape of deformed liposomes and infer quantitative mechanical properties.

## **Experimental**

### **Reagents**

All lipids were purchased from Avanti Lipids Inc. All other reagents were from Sigma Aldrich.

### **Nanopore fabrication**

Nanopore chip fabrication began with deposition of a 200 nm thick  $\text{Si}_x\text{N}_y$  film across a 500  $\mu\text{m}$  thick silicon wafer. Photolithography and standard KOH wet-etching was then used to make a 50  $\mu\text{m}$  x 50  $\mu\text{m}$  window on the silicon wafer leaving a free standing  $\text{Si}_x\text{N}_y$  membrane on the window. Nanopores were drilled in the membrane using a FEI Strata DB 235 FIB, using protocols described elsewhere<sup>5, 75</sup>.

### **Liposome production**

Liposomes were prepared by conventional extrusion method. Lipid solutions in chloroform were used to make a thin film by rotary evaporation technique. For DOPC and POPC 10 mM concentration of lipid in chloroform were used. For Cholesterol-containing liposomes (DOPC/Ch and POPC/Ch), 5mM of cholesterol in chloroform was added before evaporation. The thin films were rehydrated in Phosphate Buffer Saline (pH = 7.4) and were heated to temperature above the transition point of the lipids. The solution was then extruded using membranes with 100 nm pores and a desktop mini-extruder by Avanti Lipids Inc.

### **Particle size measurements**

The hydrodynamic diameter of all samples were measured by dynamic light scattering (DLS) in a Delsa Nano instrument by Beckman Coulter. Diluted samples in PBS were used to measure intensity-weighted diameters of analytes and Gaussian distributions were fitted to histograms to find the peaks. Each measurement was repeated 4 times and the average was used as hydrodynamic diameter of each

sample. Transmission Electron Microscopy was used to examine the shape of liposomes and nanoparticles. 10  $\mu\text{l}$  of diluted sample was dispensed on a carbon grid for 20 minutes at 4  $^{\circ}\text{C}$ . The grids were then floated on a 50  $\mu\text{l}$  drop of fixative solution (1% formaldehyde and 0.1% glutaraldehyde in PBS) at 4  $^{\circ}\text{C}$ . The grids were then washed once in PBS and several times in water by floating them over 50  $\mu\text{l}$  droplets of liquids at room temperature. Subsequently, the excess liquid was removed by wicking with a filter paper and the grids were immediately floated on a 20  $\mu\text{l}$  drop of 2% phosphotungstic acid for negative staining. The excess staining solution was wicked with filter paper after 2 minutes and the TEM sample was air dried. The sample was imaged using a JOEL 2100 TEM instrument at an operating accelerating voltage of 120 keV. A similar protocol without fixing steps was used for TEM imaging of polystyrene particles.

#### **Nanopore resistive pulse sensing**

A nanopore chip was sealed by sandwiching it between two PDMS gaskets and assembling it in an in-house built flow cell. *Cis* and *trans* chambers of the flow cells were filled with the electrolyte (PBS). A 200 B Axopatch patch-clamp amplifier by Molecular Devices was used with Ag/AgCl electrodes to record signals. The samples were then added to the *trans* chamber and the current was recorded at a sampling frequency of 250 kHz. The signal was digitized with an MD Digidata 1440A digitizer and filtered by a 10 kHz analog low-pass Bessel filter. The data for all the liposomes and polystyrene beads were recorded using the same pore shown in Figure 1a. The conductance of this pore was  $\sim 44.6$  nS. Before recording data for each new sample, the nanopore was thoroughly cleaned in piranha solution (at 80 $^{\circ}\text{C}$ ) for 10-15 minutes. The open current (electrolyte without analyte) was monitored for several minutes to ensure that the conductance of the pore was the same and no trace of contaminants from previous experiments was left in the pore or flow cells. All the experiments (except for NP120) were replicated twice. The average value of the two measurements and the standard error of the means were used to generate the plots.

### Signal processing

All signal processing and data plotting were done in MATLAB using codes and custom graphical interfaces developed in-house. For baseline correction, we used a moving average technique. For event detection, we used an iterative detection algorithm similar to what was reported by Plesa and Dekker<sup>76</sup>. For more details on signal processing and event detection see the supplementary information.

### Finite element simulation

Finite element simulation was done in COMSOL following the methods described before<sup>43</sup>. We used a 2D axisymmetric model and solved Poisson, Nernst-Planck and Navier-Stokes equations to determine electric field and ionic fluxes. For *cis* and *trans* chambers we used spheres of radius 1  $\mu\text{m}$ . The pore was modeled by a cylinder with inner diameter,  $R = 250 \text{ nm}$ , and height,  $h = 200 \text{ nm}$  to reflect the dimensions of the pore used in the experiments. The ionic current was calculated by integrating ionic fluxes through the center of the pore. The constants used for the simulation were:  $T = 298\text{K}$  for temperature;  $R = 8.31 \text{ J}/(\text{mol}\cdot\text{K})$  for gas constant;  $F = 96485.3365 \text{ C}/\text{mol}$  for Faraday constant;  $D_k = 1.957 \times 10^{-9} \text{ m}^2/\text{s}$  and  $D_{cl} = 2.032 \times 10^{-9} \text{ m}^2/\text{s}$  for diffusion coefficient of ions,  $\epsilon = 80$  for relative permittivity of water;  $\eta = 10^{-3} \text{ Pa}\cdot\text{s}$  for viscosity of water;  $\rho = 10^3 \text{ kg}/\text{m}^3$  for density of water,  $C_K = C_{Cl} = 140 \text{ mM}$  for bulk KCl concentrations;  $Z_K = 1$  and  $Z_{Cl} = -1$  for valence of  $\text{K}^+$  and  $\text{Cl}^-$  ions; and  $\sigma = -0.2 \text{ mC}/\text{m}^2$  for surface charge on the nanopore. Further details about the finite element simulations can be found in the supplementary information.

### Conclusions

We have demonstrated that nanoscale liposomes can undergo significant deformation as they translocate through a solid-state nanopore. This was confirmed by observing the change in normalized resistive pulse heights at increasing applied voltages. Based on the pulse heights, we determined that liposomes assume a prolate ellipsoid morphology, in agreement with the results from electrodeformation experiments<sup>35, 38, 39, 57, 59, 60</sup>. Finite element simulation was then employed to resolve the effective aspect ratio of deformed liposomes, which allowed us to characterize the extent of

liposome deformation. Even though the estimated aspect ratios seem uncharacteristically high, we were able to compare the qualitative elasticity of various liposomes and describe the effect of cholesterol on the rigidity of various nanoscale liposomes. In conclusion, resistive pulse sensing in solid-state nanopores can potentially characterize the mechanical rigidity of nanoscale liposomes. Accurate quantitative measurements require further in depth analysis of the underlying physics, theoretical modeling of liposome electrodeformation, as well as optimization of the experimental technique in several fronts beyond the scope of this work, yet the findings here can collectively serve as the proof-of-the-principle and lay down the framework for future studies.

The work in this paper can be of great significance for researches in various fields including nanopore sensing technology, vesicle characterization and cellular/molecular mechanobiology. Particularly for nanopore sensing, it is important to understand the deformation of soft nanoparticles and the implications for nanoparticle characterization such as counting and size measurements. As we demonstrated in this paper, the shape of liposomes inside nanopores can be very different from that in bulk solution, which can influence the size measurement. Generally, one should be cautious about estimating the size of particles from resistive pulse signals as the shape can have a significant influence on the results. We suggest that resistive pulse sensing should always be compared at varied applied voltages to confirm no artifact caused by deformation and if possible sample preparation methods such as fixation, etc. should be used to minimize the effects of deformation.

### **Acknowledgements**

This work was supported by National Science Foundation (CMMI #1435000 and #1562505) and National Research Foundation of Korea (GRDC NRF-2015K1A4A3047100 and NRF-2015M3A7B6027973). The authors are grateful to Dr. Irwin Chaiken at Drexel University College of Medicine for use of his laboratory facilities and helpful discussion.

**Notes and references**

1. A. J. Storm, J. H. Chen, X. S. Ling, H. W. Zandbergen and C. Dekker, *Nat. Mater.*, 2003, **2**, 537-540.
2. M. Wanunu, *Phys. Life. Rev.*, 2012, **9**, 125-158.
3. J. B. Edel and T. Albrecht, *Engineered nanopores for bioanalytical applications*, William Andrew, 2013.
4. D. W. Deamer and D. Branton, *Acc. Chem. Res.*, 2002, **35**, 817-825.
5. M. J. Kim, M. Wanunu, D. C. Bell and A. Meller, *Adv. Mater.*, 2006, **18**, 3149-3153.
6. M. Wanunu, T. Dadosh, V. Ray, J. Jin, L. McReynolds and M. Drndic, *Nat. Nanotechnol.*, 2010, **5**, 807-814.
7. B. M. Venkatesan and R. Bashir, *Nat. Nanotechnol.*, 2011, **6**, 615-624.
8. D. Fologea, B. Ledden, D. S. McNabb and J. Li, *Appl. Phys. Lett.*, 2007, **91**, 539011-539013.
9. B. Ledden, D. Fologea, D. S. Talaga and J. Li, in *Nanopores*, eds. S. M. Iqbal and R. Bashir, Springer, 2011, pp. 129-150.

10. R. Wei, V. Gatterdam, R. Wieneke, R. Tampe and U. Rant, *Nat. Nanotechnol.*, 2012, **7**, 257-263.
11. D. K. Kwak, H. Chae, M. K. Lee, J. H. Ha, G. Goyal, M. J. Kim, K. B. Kim and S. W. Chi, *Angew. Chem. Int. Ed.*, 2016.
12. J. D. Uram, K. Ke, A. J. Hunt and M. Mayer, *Small*, 2006, **2**, 967-972.
13. N. Arjmandi, W. Van Roy, L. Lagae and G. Borghs, *Anal. Chem.*, 2012, **84**, 8490-8496.
14. A. McMullen, H. W. de Haan, J. X. Tang and D. Stein, *Nat. Commun.*, 2014, **5**, 4171.
15. A. S. Prabhu, T. Z. Jubery, K. J. Freedman, R. Mulero, P. Dutta and M. J. Kim, *J. Phys. Condens. Matter.*, 2010, **22**, 454107.
16. M. Davenport, K. Healy, M. Pevarnik, N. Teslich, S. Cabrini, A. P. Morrison, Z. S. Siwy and S. E. Letant, *ACS Nano*, 2012, **6**, 8366-8380.
17. G. Goyal, K. J. Freedman and M. J. Kim, *Anal. Chem.*, 2013, **85**, 8180-8187.
18. S. Liu, T. D. Yuzvinsky and H. Schmidt, *ACS Nano*, 2013, **7**, 5621-5627.
19. Y. Rudzevich, Y. Q. Lin, A. Wearne, A. Ordonez, O. Lupan and L. Chow, *Colloids Surf. A*, 2014, **448**, 9-15.

20. R. E. Lane, D. Korbie, W. Anderson, R. Vaidyanathan and M. Trau, *Sci. Rep.*, 2015, **5**, 7639.
21. N. Arjmandi, W. Van Roy and L. Lagae, *Anal. Chem.*, 2014, **86**, 4637-4641.
22. K. Zhou, L. Li, Z. Tan, A. Zlotnick and S. C. Jacobson, *J. Am. Chem. Soc.*, 2011, **133**, 1618-1621.
23. S. L. Maas, J. de Vrij, E. J. van der Vlist, B. Geragousian, L. van Bloois, E. Mastrobattista, R. M. Schiffelers, M. H. Wauben, M. L. Broekman and E. N. Nolte-'t Hoen, *J. Control. Release*, 2015, **200**, 87-96.
24. S. van Dorp, U. F. Keyser, N. H. Dekker, C. Dekker and S. G. Lemay, *Nat. Phys.*, 2009, **5**, 347-351.
25. J. B. Heng, A. Aksimentiev, C. Ho, P. Marks, Y. V. Grinkova, S. Sligar, K. Schulten and G. Timp, *Biophys. J.*, 2006, **90**, 1098-1106.
26. K. J. Freedman, M. Jurgens, A. Prabhu, C. W. Ahn, P. Jemth, J. B. Edel and M. J. Kim, *Anal. Chem.*, 2011, **83**, 5137-5144.
27. A. Oukhaled, B. Cressiot, L. Bacri, M. Pastoriza-Gallego, J. M. Betton, E. Bourhis, R. Jede, J. Gierak, L. Auvray and J. Pelta, *ACS Nano*, 2011, **5**, 3628-3638.
28. K. J. Freedman, S. R. Haq, J. B. Edel, P. Jemth and M. J. Kim, *Sci. Rep.*, 2013, **3**, 1638.

29. D. S. Talaga and J. Li, *J. Am. Chem. Soc.*, 2009, **131**, 9287-9297.
30. G. Oukhaled, J. Mathe, A. L. Biance, L. Bacri, J. M. Betton, D. Lairez, J. Pelta and L. Auvray, *Phys. Rev. Lett.*, 2007, **98**, 158101.
31. M. Pevarnik, M. Schiel, K. Yoshimatsu, I. V. Vlassiuk, J. S. Kwon, K. J. Shea and Z. S. Siwy, *ACS Nano*, 2013, **7**, 3720-3728.
32. D. A. Holden, J. J. Watkins and H. S. White, *Langmuir*, 2012, **28**, 7572-7577.
33. R. Dimova, K. A. Riske, S. Aranda, N. Bezlyepkina, R. L. Knorr and R. Lipowsky, *Soft Matter*, 2007, **3**, 817-827.
34. M. Kummrow and W. Helfrich, *Phys. Rev. A*, 1991, **44**, 8356-8360.
35. R. S. Gracia, N. Bezlyepkina, R. L. Knorr, R. Lipowsky and R. Dimova, *Soft Matter*, 2010, **6**, 1472-1482.
36. M. M. Sadik, J. Li, J. W. Shan, D. I. Shreiber and H. Lin, *Phys. Rev. E*, 2011, **83**, 066316.
37. P. F. Salipante, R. L. Knorr, R. Dimova and P. M. Vlahovska, *Soft Matter*, 2012, **8**, 3810-3816.
38. L. C. McConnell, M. J. Miksis and P. M. Vlahovska, *IMA J. Appl. Math.*, 2013, **78**, 797-817.

39. P. F. Salipante and P. M. Vlahovska, *Soft Matter*, 2014, **10**, 3386-3393.
40. G. Goyal, A. Darvish and M. J. Kim, *Analyst*, 2015, **140**, 4865-4873.
41. M. Tsutsui, Y. He, K. Yokota, A. Arima, S. Hongo, M. Taniguchi, T. Washio and T. Kawai, *ACS Nano*, 2016, **10**, 803-809.
42. R. DeBlois and C. Bean, *Rev. Sci. Instrum.*, 1970, **41**, 909-916.
43. T. Z. Jubery, Prabhu, A. S., Kim, M. J., Dutta, P., *Electrophoresis*, 2012, **33**, 325-333.
44. K. E. Venta, M. B. Zanjani, X. Ye, G. Danda, C. B. Murray, J. R. Lukes and M. Drndic, *Nano Lett.*, 2014, **14**, 5358-5364.
45. W. J. Lan, D. A. Holden, B. Zhang and H. S. White, *Anal. Chem.*, 2011, **83**, 3840-3847.
46. Y. Ai, M. K. Zhang, S. W. Joo, M. A. Cheney and S. Z. Qian, *J. Phys. Chem. C*, 2010, **114**, 3883-3890.
47. M. Mao, NORTHWESTERN UNIVERSITY, 2015.
48. J. B. Heng, A. Aksimentiev, C. Ho, P. Marks, Y. V. Grinkova, S. Sligar, K. Schulten and G. Timp, *Nano Lett.*, 2005, **5**, 1883-1888.

49. D. A. Holden, G. Hendrickson, L. A. Lyon and H. S. White, *J. Phys. Chem. C*, 2011, **115**, 2999-3004.
50. M. Firnkes, D. Pedone, J. Knezevic, M. Doblinger and U. Rant, *Nano Lett.*, 2010, **10**, 2162-2167.
51. H. Aihara and J. Miyazaki, *Nat. Biotechnol.*, 1998, **16**, 867-870.
52. G. Chu, H. Hayakawa and P. Berg, *Nucleic Acids Res.*, 1987, **15**, 1311-1326.
53. M. R. Prausnitz, V. G. Bose, R. Langer and J. C. Weaver, *Proc. Natl. Acad. Sci. USA*, 1993, **90**, 10504-10508.
54. T. Y. Tsong, *Biophys. J.*, 1991, **60**, 297-306.
55. R. Dimova, *Adv. Colloid Interface Sci.*, 2014, **208**, 225-234.
56. J. Chen, M. Abdelgawad, L. M. Yu, N. Shakiba, W. Y. Chien, Z. Lu, W. R. Geddie, M. A. S. Jewett and Y. Sun, *J. Micromech. Microeng.*, 2011, **21**.
57. R. Dimova, N. Bezlyepkina, M. D. Jordo, R. L. Knorr, K. A. Riske, M. Staykova, P. M. Vlahovska, T. Yamamoto, P. Yang and R. Lipowsky, *Soft Matter*, 2009, **5**, 3201-3212.
58. L. C. McConnell, P. M. Vlahovska and M. J. Miksis, *Soft Matter*, 2015, **11**, 4840-4846.

59. S. Kakorin, T. Liese and E. Neumann, *J. Phys. Chem. B*, 2003, **107**, 10243-10251.
60. V. Dimitrov, S. Kakorin and E. Neumann, *Phys. Chem. Chem. Phys.*, 2013, **15**, 6303-6322.
61. K. A. Riske and R. Dimova, *Biophys. J.*, 2006, **91**, 1778-1786.
62. K. A. Riske and R. Dimova, *Biophys. J.*, 2005, **88**, 1143-1155.
63. F. Tokumasu, A. J. Jin, G. W. Feigenson and J. A. Dvorak, *Ultramicroscopy*, 2003, **97**, 217-227.
64. G. Puu and I. Gustafson, *Biochim. Biophys. Acta.*, 1997, **1327**, 149-161.
65. K. Kumar, L. Isa, A. Egner, R. Schmidt, M. Textor and E. Reimhult, *Langmuir*, 2011, **27**, 10920-10928.
66. N. Delorme and A. Fery, *Phys. Rev. E Stat. Nonlin. Soft Matter Phys.*, 2006, **74**, 030901.
67. J. C. Stachowiak, F. M. Brodsky and E. A. Miller, *Nat. Cell. Biol.*, 2013, **15**, 1019-1027.
68. S. Li, F. Eghiaian, C. Sieben, A. Herrmann and I. A. Schaap, *Biophys. J.*, 2011, **100**, 637-645.

69. O. Soubias, W. E. Teague, Jr., K. G. Hines, D. C. Mitchell and K. Gawrisch, *Biophys. J.*, 2010, **99**, 817-824.
70. N. Kucerka, S. Tristram-Nagle and J. F. Nagle, *J. Membr. Biol.*, 2005, **208**, 193-202.
71. J. Henriksen, A. C. Rowat, E. Brief, Y. W. Hsueh, J. L. Thewalt, M. J. Zuckermann and J. H. Ipsen, *Biophys. J.*, 2006, **90**, 1639-1649.
72. J. Pan, S. Tristram-Nagle and J. F. Nagle, *Phys. Rev. E Stat. Nonlin. Soft Matter Phys.*, 2009, **80**, 021931.
73. J. L. Fraikin, T. Teesalu, C. M. McKenney, E. Ruoslahti and A. N. Cleland, *Nat. Nanotechnol.*, 2011, **6**, 308-313.
74. M. Mayer, *Biophys. J.*, 2015, **108**, 490a-490a.
75. G. Goyal, R. Mulero, J. Ali, A. Darvish and M. J. Kim, *Electrophoresis*, 2015, **36**, 1164-1171.
76. C. Plesa and C. Dekker, *Nanotechnology*, 2015, **26**, 084003.

## FIGURES

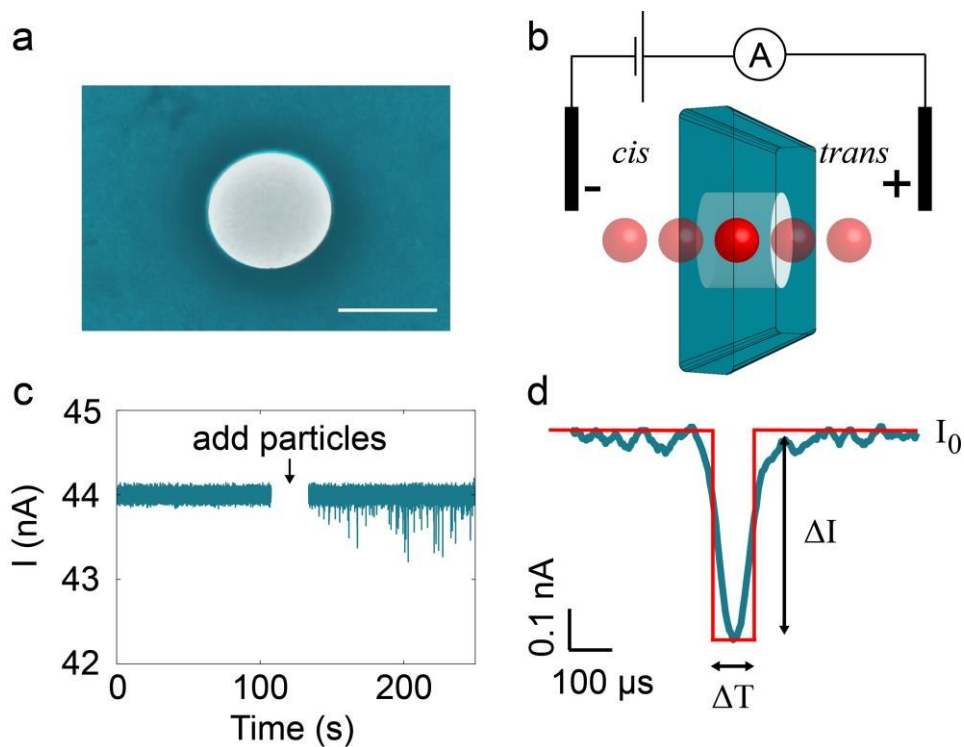


**Figure 1.** (a) Pseudo-colored TEM image of a nanopore 250 nm in diameter, drilled in a 200 nm thick silicon nitride membrane. (b) Schematic illustration of nanopore resistive pulse sensing. Two Ag/AgCl electrodes were used to apply a bias voltage across the pore and temporal changes in the ionic current through the pore was recorded during particle translocation. (c) Example of ionic current measurement with phosphate buffer saline solution before and after adding liposomes at an applied voltage of 1 V. (d) Magnified view of a single resistive pulse in (c);  $I_0$  is the baseline current;  $\Delta I$  and  $\Delta T$  denote the height and the full width at half maximum of the signal, respectively.

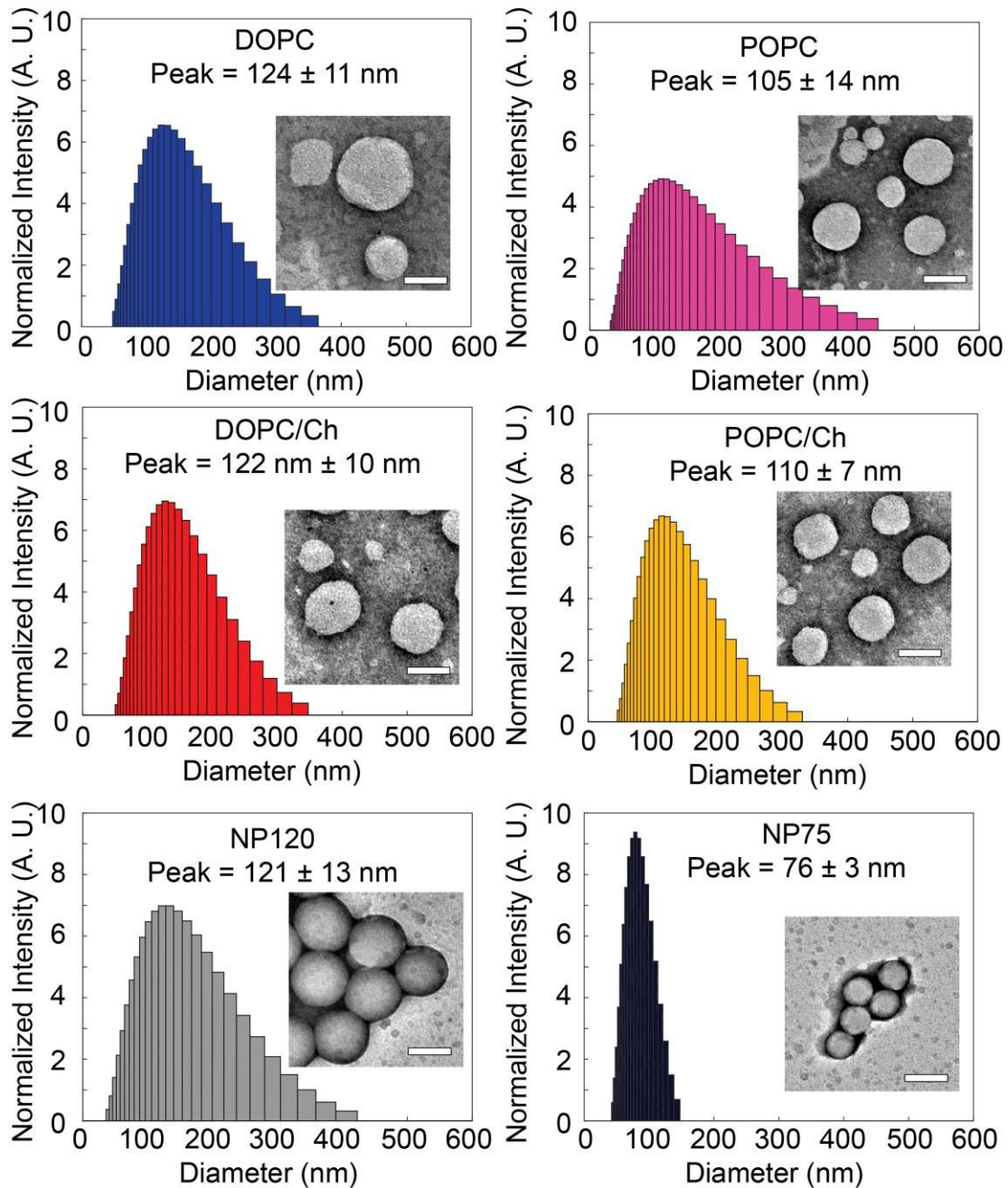


**Figure 2.** Size distribution of particles measured by dynamic light scattering as well as TEM images of each sample. All scale bars are 100 nm.

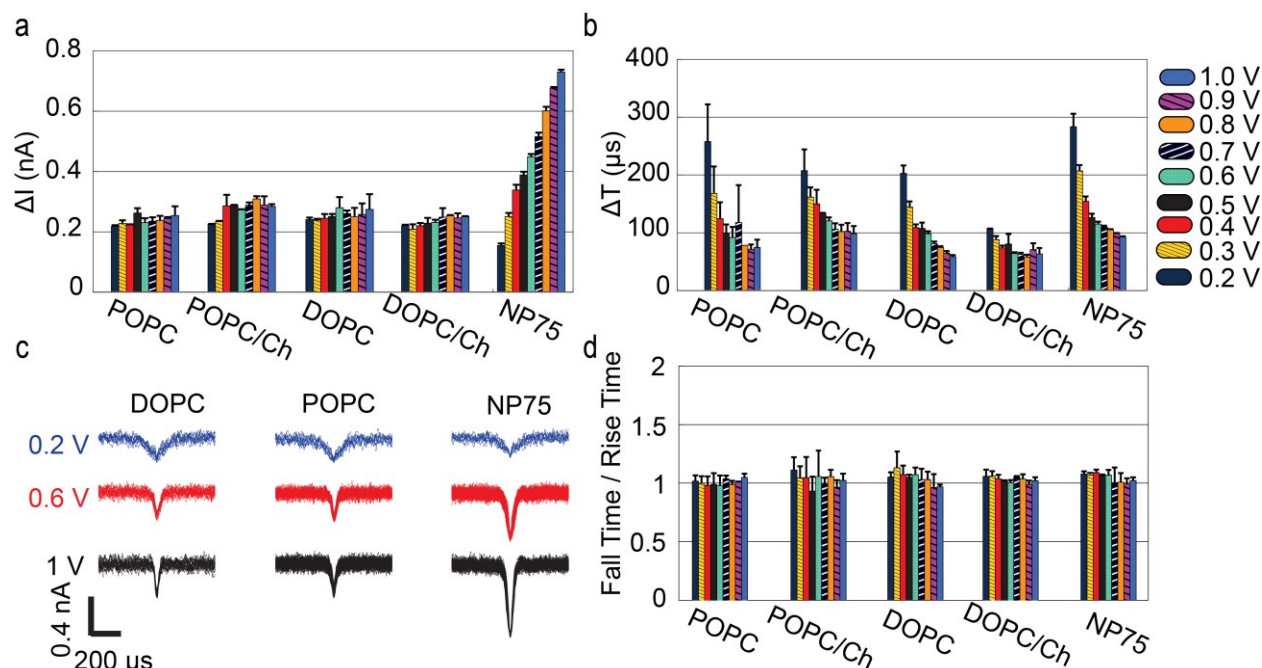


**Figure 3.** Dependence of resistive pulses on applied voltage. (a) Most probable amplitude of resistive pulse ( $\Delta I$ ) for liposomes and 75nm polystyrene nanoparticles at varied applied voltages. As depicted by the legend in the right, the bars from left to right represent an applied voltage of 0.2-1 V with an interval of 0.1V). (b) Most probable translocation time (c) Overlay of more than 100 resistive pulse traces at low (0.2 V), mid (0.6 V) and high (1V) applied voltages for DOPC, POPC and NP75. (d) The average rise time to fall time ratio of resistive pulses for all samples. All error bars are the standard error of the means from two replicate experiments.

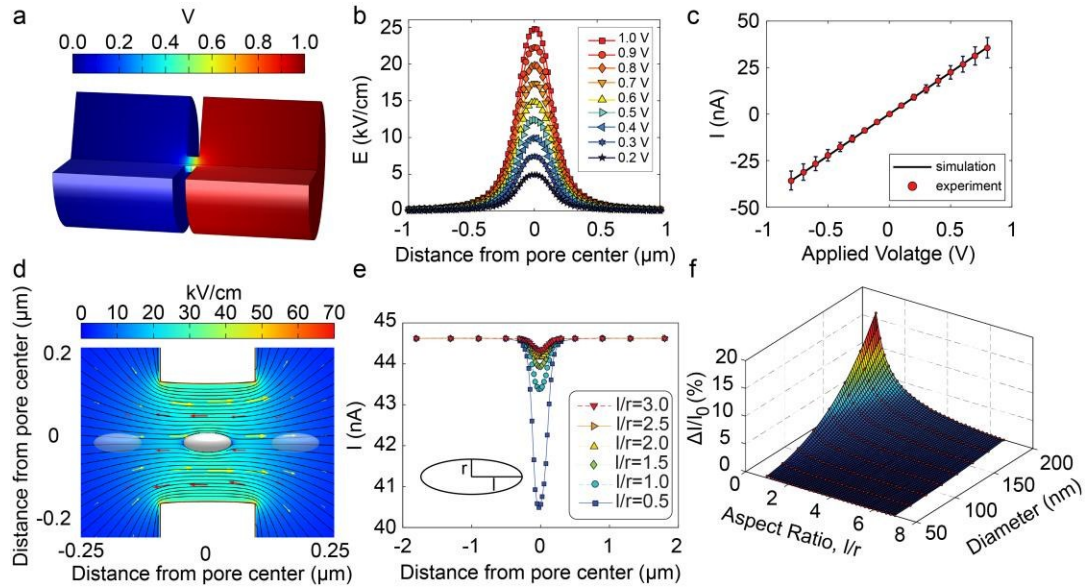


**Figure 4.** Numerical simulation of nanopore conductance; (a) Voltage distribution around a nanopore. (b) Magnitude of the electric field inside the pore; The x-axis shows the distance from the center of the pore on the pore axis. (c) Comparison of open pore conductance between simulation and experiments; black line shows the simulation, and red dots show the experimental data. Error bars show standard error in 5 replicate measurements. (d) Translocation of an elliptical particle through the center of the pore. The color gradient shows the magnitude of the electric field inside the pore, when the particle is at the center of the pore and the black lines show the field streamlines. The yellow and red arrows show the flux of negatively charge,  $\text{Cl}^-$ , ions and positively charged,  $\text{K}^+$ , ions, respectively. (e) Simulated resistive pulse for elliptical particles of different aspect ratios; Oblate ellipsoids ( $l/r < 1$ ), spheres ( $l/r = 1$ ) and prolate ellipsoids ( $l/r > 1$ ) are compared. (f) Comparison of the simulated normalized current blockade ( $\Delta I/I_0$ ) for elliptical particles with varied size and aspect ratios. Red dots show the simulated data points from the model and the color gradient surface shows the intermediate values calculated by cubic polynomial fitting.

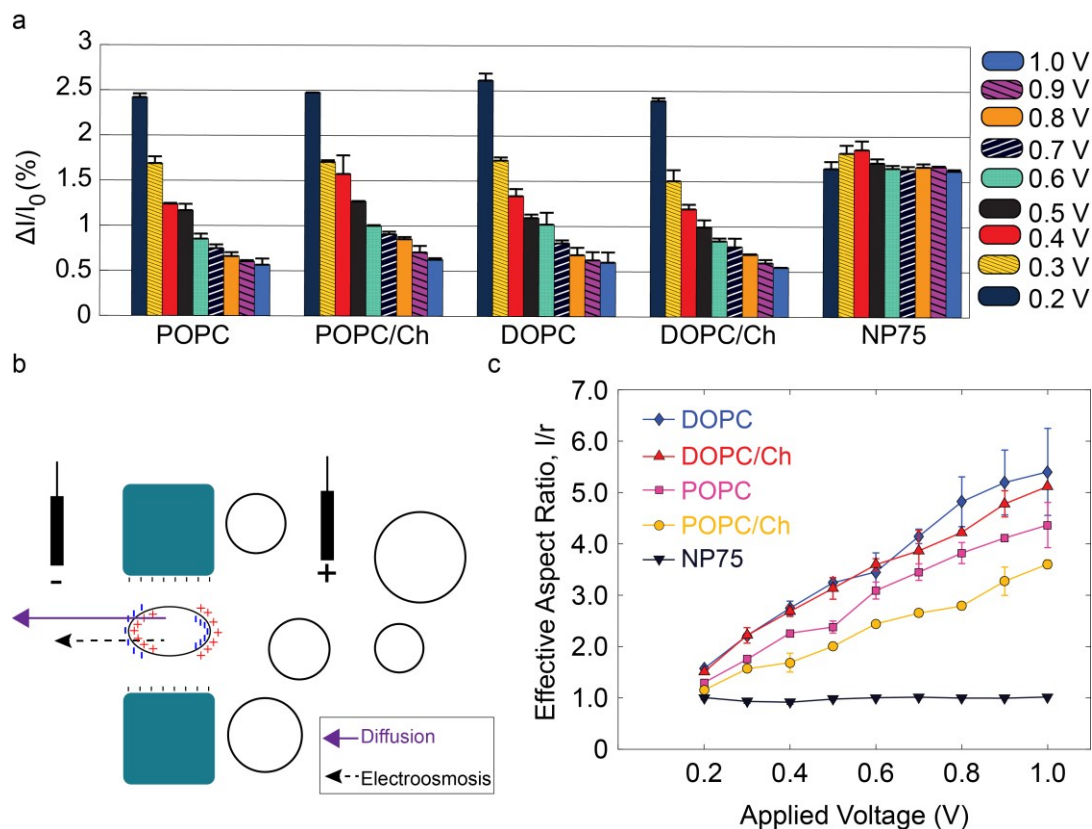


**Figure 5.** (a) normalized current blockade for all samples at varied applied voltages. As shown in the legend, the bars from left to right show an applied voltage of 0.2V to 1V with an interval of 0.1V. The error bars show standard error from experiments replicated twice. (b) Liposomes get charged inside nanopores but the net electrophoretic force on liposomes is zero. Since the liposomes were placed in the *trans* chamber, diffusion and electroosmotic flow are in the same direction (c) The effective aspect ratio is estimated for all samples based on the normalized current blockade and the numerical simulation results.